Physiochemical effect on the microgroove microstructure in microcutting of pure copper

Jiayi Zhang (jiayizhang21@jxust.edu.cn)
Jiangxi University of Science and Technology

Research Article

Keywords: physiochemical effect, microcutting, microgroove, texture, recrystallization

Posted Date: November 2nd, 2021

DOI: https://doi.org/10.21203/rs.3.rs-960942/v2

Abstract

The physiochemical effect on the microcutting of pure copper is studied through characterization on the cross-sectioned microgroove. An obvious reduction in cutting force and thrust force can be obtained with the application of ink surfactant. The surface roughness of microgroove with physiochemical effect is 12 nm, and that without physiochemical effect is 17 nm. The average grain size of the ink-affected sample is 67.9 μm within the microgroove zone, and that of the ink-free sample is 48.3 μm within the microgroove zone, moreover, the grain size of ink-free microgroove near the microgroove surface is larger than that far away from the microgroove surface. Additionally, the grain orientations of ink-affected cross-sectioned surface present anisotropy, while that of ink-free cross-sectioned surface are towards {101} direction. Based on the calculation and analysis of geometrically necessary dislocation, it can be inferred that the induced stress and temperature in the sample with physiochemical effect are higher than that without physiochemical effect, which can provide enough driving energy for recrystallization.

1. Introduction

Ultraprecision microcutting began in the middle of 21th century for electronics, energy and national defense applications to produced nano-scale finishing and submicron shape precision in complex structures. To date, with the high accuracy resolution ranging from 5–50 nm, the advantages for applications expand to the biomedicine (Yi et al. 2008), electronics (Tan and Guo, 2018) and optical fields (Otieno and Dornfield, 2008), including a wider range of engineering materials, aluminum, copper, titanium and additive manufacturing alloys.

Presently, there has been an incremental research interest in the application of surfactants to improve the performance of metal machining, which significantly improve the machined surface quality (Sagaouram and Udupa, 2018). Surfactants play an important role in microcutting process to enhance the heat dissipation generated by friction and support chip transfer from the machining zone. The application of surfactants causing surface adsorption phenomena, which varies from embrittlement to plasticization, such as the Kramer, Roscoe, and Rehbinder effects (Kramer, Roscoe and Renbinder, 1928). The most studied physiochemical phenomenon on metal microcutting is the Rehbinder effect (R-effect), which means the reduction in surface energy and crack growth of the metal surface by chemical adsorption. During microcutting, the decreased surface energy usually leads to macro variations, such as sharp reduction of cutting force, and chip morphologies change. In the early tears, Shaw (1958) used carbon tetrachloride as a cutting fluid during metal machining, and observed the half chip thickness and cutting forces, accompanied with improved surface roughness. More recently, Zhang et al. (2021) also found a reduction in cutting and thrust forces with the application of ink during microcutting of AA 6061 alloy, and observed thick cutting chip for ink-free sample and thin cutting chip for ink-affected sample. For years, a lot of research has been done on the chip morphology affected by surface active medium during metal cutting process. However, there is no significant progress on the R-effect on machined surface except for microstructure characteristics. The surface active medium has a dramatic effect on the

machinability of metals, thus it is necessary to study the R-effect on the material characteristics of the machined surface.

In fact, microcutting process is equivalent to plastic deformation process. Due to the instability of heat generation, the microstructure of the deformation zone can be affected, such as dislocation, precipitates, grain size and texture. However, at present, there are few studies on the influence of microcutting on the morphology and properties of microgrooves. It can be learned from the influence of other deformation modes on the morphology of metals, so as to understand its importance. Wang et al. (2015) reported that the cold-deformation in Al-Mg-Si-Cu alloy made texture variations obviously, from Cube texture to Cube and P textures. Peirs et al. (2013) observed recrystallized grains (~100 nm in size) existed in the core of deformation bands in Ti6Al4V alloy, accompanied with twins and a needle-like martensitic near the deformation zones. Zhang et al. (2018) also found that extrusion and drawing process generate β" precipitates, and the numerous subgrains and high densities of the dislocations accelerated the formation of abundant dispersive nano-sized β" precipitates.

Since the effect of surfactants on the properties of deformed metals, physiochemical effects post an interesting scientific issues for machined surfaces, especially with regard to grains, dislocations, and textures. According to the existed studies, few studies have clarified the influence of physiochemical effect on the microstructures of the machined surface and microgroove in metals. Therefore, the aim of this study is to investigate the physiochemical effect on microstructure and surface roughness of microgrooves in pure copper. It is helpful to understand the microstructure variations of microgroove under physiochemical effect during the microcutting process.

2. Experiments

Microcutting experiments were carried out on a Toshiba ULG 100 ultraprecision machine with a single crystal diamond cutting tool with a nose radius of 0.8 mm. The schematic diagram is listed in the previous paper (Zhang et al. 2021), and also shown in Fig. 1 for more intuitive representation. The pure copper was selected for the microcutting experiments, and this was done to avoid too much defects and phases influencing machining process. Before microcutting experiments, turning was carried out on the end face to ensure its smoothness and accuracy alignment with the diamond tool. Subsequently, a permanent metal marker ink was applied on half of the surface before microcutting tests. The cross-sectioned microgroove areas were marked as Sample A (without R-effect) and Sample B (with R-effect). The microcutting parameters were set as 25 and 100 mm/min for cutting speed, respectively, and 10 μm for cutting depth. The machining forces were tested on a Kistler 9256C1 dynamometer and Type 5051 amplifiers at the frequency of 10 kHz. An Olympus 3D laser scanning confocal microscope was employed to test surface roughness of microgrooves and then the permanent metal marker ink was removed from the surface by ethyl alcohol. Afterwards, the microgrooves of Samples A and B were treated by ion thinning for electron backscattered diffraction (EBSD) analysis from the cross section view of the microgrooves, using an FEI Helios Nanolab 600i focused ion beam (FIB)/ scanning electron microscope (SEM) system with an accelerating voltage of 20 kV. The grain size, orientation distribution

function (ODF), texture and geometrical necessary dislocations were calculated using Channel 5 and ATEX software.

3. Results

3.1 The tested machining forces of the Samples

The machining forces captured in microcutting are presented in Fig. 2. Obviously, the cutting and thrust forces drastically decrease for the ink-affected microgrooves during microcutting. The average cutting force of Sample A is 3.69 N, and that of Sample B is 2.37 N, displaying an evident reduction in Sample B at 25 mm/min cutting speed. For 100 mm/min cutting speed, the average cutting force of Sample A is 3.15 N, and that of Sample B is 2.21 N. Moreover, the cutting and thrust forces variations are more stable and display an evident reduction in the Sample B, these phenomenon further confirms the induction of physiochemical effect with ink during microcutting. Interestingly, it can be found that physiochemical effect is more obvious at 25 mm/min cutting speed, that is, the difference of machining forces (cutting and thrust forces) between Sample A and B is more evident. Previous study reported that the R effect is more pronounced at lower cutting depth (1 μm) (Zhang et al. 2020). Thus, it can be deduced that low cutting speed and cutting depth are favorable to induce physiochemical effect.

3.2 Surface roughness of the microgrooves after microcutting

To scan more areas of surface roughness, the ink-free and ink-affected samples with cutting depth 10 μm were selected for 3D laser scanning confocal microscope to measure surface roughness. Fig. 3 presents the surface quality maps and roughness of the machined surfaces. Fig. 3 (a) presents the rough machined surface containing voids of the Sample A. As for Fig. 3 (b), an obvious improvement surface roughness can be observed, and less voids were formed on the machined surface of Sample B (with physiochemical effect). According to the measurement, the surface roughness (*R*a) of Sample A is 17 nm, while that of Sample B is 12 nm. This big difference in surface roughness validate the existence of physiochemical effect during microcutting of pure copper, which sets the foundation for the reasoning of the subsequent EBSD analyses.

3.3 The microstructures of cross-sectioned microgrooves

Fig. 4 shows the EBSD mapping of the cross-sectioned microgrooves of Sample A and B, presenting the difference of microstructure between the two samples. Fig. 4 (a) displays grains averaging 48.3 μm in size within the microgroove zone. Notably, the grains near the surface (marked as white dotted line) of the microgrooves are finer, about 28 μm. Some of these grains oriented towards {101} direction. The grains far away from the microgroove surface (distance about 25μm) have larger size, about 60 μm, and represent obvious anisotropy, indicating that microcutting process and movement of cutting tool do not affect these grains. In contrast, the average grain size of Fig. 4 (b) is 67.9 μm within the microgroove zone, and the grain size near the ink-affected microgroove surface is larger than that near the ink-free microgroove. Interestingly, the distance between the affected grains (marked as yellow dotted line) and the microgroove surface is 61.3 μm, which may means the range of the affected grains is larger due to

the physiochemical effect, or the grains are not affected by the physiochemical effect at all, because the grain size is similar to that far away from the surface. Additionally, the grain orientations of ink-affected microgroove surface present anisotropy. Thus, according to the above phenomena, two conjectures are put forward: the grains with physicochemical effect recrystallize after heat generation by microcutting deformation, and then some grains grow up; the grains are not affected by physiochemical effect during microcutting.

Fig. 5 displays the Schmid factor maps for each individual grain in the two microgroove zones of the samples. A lower Schmid factor indicates the high deformation resistance of the grain. In Sample A (Fig. 5 (a)), the Schmid factor of the grains near the surface ranges from 0.25 to 0.43, and that far away from the surface is almost around 0.4. Thus it can be deduced that the some grains near the microgroove surface are deformed during microcutting, and the grains far away from the surface are slightly influenced. As for the Sample B (Fig. 5 (b)), the Schmid factors of the grains near the surface retain at 0.42, which are close to that of the grains far away from the surface. However, the Schmid factor of one grain far away from the surface is 0.23, which is quite different from the nearby Schmid factor. It may be considered that the microcutting with physiochemical effect may deeply affect the internal grains, thus it is preliminarily inferred that the grains near the surface are composed of many fine subgrains after recrystallization.

The clear differences in grain size and Schmid factor evolution after microcutting imply that the textures may also be affected by physiochemical effect. Fig. 6 presents the ODF maps for grains in the cross-sectioned microgroove zones of the samples. It can be known that {110}<001>, {110}<112>, {111}<110> and {123}<634> textures dominate in Sample A, and {110}<112>, {112}<111> and {124}<211> textures dominate in Sample B. {112}<111> texture is present in Sample A and B, which may indicate this texture will not be affected by physiochemical effect. Zhang et al. (2018) explained that <111> orientated grains had internal recrystallization energy storage at annealing processes, recrystallization might occur. Thus, based on this study, it may be inferred that grains of Sample B may have recrystallized after microcutting. At $\phi 2 = 0°$, {112}<111> is observed for Sample A and B, and that in Sample B has higher intensity than that in Sample A. At $\phi 2 = 45°$, Sample B has high intensity of {110}<112> while invisible in the Sample A. At $\phi 2 = 65°$, Sample A has high intensity of {123}<623> texture and Sample B has high intensity of {124} <211> texture.

The volume fraction for texture of the two samples are presented in Table 1. The highest texture volume fraction is the {112}<111> texture (17.3 %) and {110}<112> texture (28.9%) of Sample A and B, respectively. The volume fractions of {110}<001> and {110}<112> textures increase with the decreased {111}<110> and {123}<634> textures under the physiochemical effect. From the view of the texture variations, it can be deduced that some of the textures will be transformed due to the physiochemical effect. Some research reported that {011}<100> texture is stable (Shen et al. 2016), and {112} <111> texture is normally generated at the deformed structures (Zhang et al. 2019). Thus, according to these research, it can be deduced that partial deformed structures exist in the Sample A and B, and the Sample B may has stable microstructure due to the appearance of {011}<100> stable texture.

Table 1
Volume fractions of textures for the two samples.

Sample	Volume fraction (%)					
	{110}<001>	{110}<112>	{111}<110>	{123}<634>	{112}<111>	{124}<211>
A	2.6	5.9	14.1	11.2	17.3	14.6
B	10.8	28.9	3.2	4.5	19.6	18.4

4. Discussion

4.1 Temperature and stress factors on microgroove microstructures

Actually, the microcutting is a plastic deformation process, which produces high stress concentration and temperature, leading to a certain degree of material recovery and recrystallization. Roland [20] referred that different strain rates will result in different stress concentration, thereby forming different deformed bands. Although many research works often relate temperature with plastic deformation, the actual temperature and stress are transient and difficult to measure. Based on this study, from the different Schmid factors of the grains, indicating that grains are affected by different stress and the localized temperature gradient, which flows into the subsurface to induce deformed substructures or recrystallization. The temperature rise (ΔT) caused by microcutting can be based on Eq. 1 (Chang, Yin and Guo, 2019):

$$\Delta \mathrm{T} = \beta \frac{\tau \gamma}{\rho C_p} \quad (1)$$

where ρ is the material density, C_p is heat capacity of the material, β is the Taylor-Quinney factor, τ is the stress, and γ is the strain. The temperature rise is strongly influence by τ and γ. τ can be taken as the stress of the sample through Taylor factor (3.06), and γ can be measured through the microstructure, which is related to the angle between the deformed zone and microcutting direction. Based on this equation, it can be inferred that the temperature rise should be determined by the stress.

To find out whether recrystallization occurs in some areas of microgrooves, and to verify the two conjectures mentioned in Section 3.3, Fig. 7 depicts the average misorientation maps of Sample A and B, which can explain directly the recrystallization degree. Generally, deformed subgrains are surrounded by low angle grain boundaries (LAGBs) ($2° < \theta < 15°$), and recrystallized subgrains are accompanied by high angle grain boundaries (HAGBs) ($\theta \geq 15°$). From the Fig. 7 (a), average misorientation distribution is uniform, and the Fig. 7 (b) shows the inhomogeneity of average misorientation. The areas close to the microgroove are delineated (marked in white dotted line), because the areas are close to the machine tool,

it is more affected by the tool friction and temperature, and the HAGBs fractions of the average misorientations in this region are calculated: 75.7 % for the Sample A and 87.4 % for the Sample. The higher fractions of HAGBs, the more recrystallized subgrains occur, obviously, recrystallized grains occupy majority for the microstructures of the Sample B. Combined with Eq. (1), it can be inferred that the induced stress and temperature in Sample B are higher than that in Sample A, which can provide enough driving energy for recrystallization.

4.2 The influence of microcutting with physiochemical effect on dislocations

There is no doubt that the shape and number of dislocations will change during the deformation process. Geometrically necessary dislocation (GND) is linked to the strain gradient filed due to geometrical constraints of the crystal lattice. When alloys are subjected to non-homogeneous plastic deformation, the corresponding strain gradient generate GND in order to keep continuity in the crystal (Liu et al. 2012). It is well known that microcutting process is often accompanied by recovery and recrystallization of grains, resulting in variations of the strain gradient. EBSD measurements can help identify crystallographic orientation, and the lattice curvature can also be calculated. Dislocations are line defects resulting in relative displacements of the crystalline lattice. The dislocation density tensor (**α**) described by Nye (1953):

$$a_{ij} = \sum_t b_i^t l_j^t \delta(\overrightarrow{x} - \overrightarrow{x}^t)$$

2

Where $\overrightarrow{l}^t$ is the dislocation direction, $\overrightarrow{b}^t$ is the displacement of Burgers vector, $\delta_{ij}$is unit tensor, $\overrightarrow{x}^t$ is a position vector. The lattice curvature tensor (**κ**) can be in introduced by lattice rotation vector θ [26]:

$$\kappa_{ij} = \frac{\partial \theta_i}{\partial x_j} = \theta_{ij}$$

3

GND is linked to heterogeneous elastic strain fields and curvatures, owing to the absence of elastic strains (ε_{ki}), the simplified equation to Nye's relations (Kröner and Balian, 1981):

$$\alpha_{ij} = \kappa_{ki} - \delta_{ki}\kappa$$

4

$$\kappa_{ki} = \alpha_{ik} - \frac{1}{2}\delta_{ki}\alpha_{mm}$$

5

The orientation of a crystalline lattice is described by the rotation, which is required to achieve the particular orientation from a chosen reference orientation. The difference of orientation between two

orientations is similarly defined by the rotation required to obtain one orientation from the other and is introduced by a disorientation angle$\Delta\theta$and rotation axis$\Delta\overrightarrow{x}$. The disorientation vector can be derived from the two adjacent orientations, from the disorientation matrix $\Delta g = (g_A)^{-1} g_B$as:

$$\Delta\theta_\kappa = -\varepsilon_{kij}\Delta g_{ij}\frac{\Delta\theta}{2\sin\Delta\theta}$$

6

As regards to the disorientation between two adjacent orientations separated spatially by$\Delta\overrightarrow{x}$, the lattice curvatures is calculated as follows:

$$\kappa_{kl} = \frac{\partial\theta_k}{\partial x_l} \approx \frac{\Delta\theta_k}{\Delta x_l}$$

7

Since local lattice orientations are resolved only in the plane (x_1 and x_2) of investigation not perpendicular to x_3. Only the six components $\kappa_{i1}$and κ_{i2}(i=1, 2, 3) of the curvature tensors are obtained but impossible for the components κ_{i3} as differentiation along the third direction.

Thus, based on this calculations of ATEX software, the GND maps of the Sample A and B are shown in Fig. 8. From the GND distribution maps, it can be deduced that GND mainly distributes at grain boundaries, certainly, it is well known that dislocations tend to submerge at grain boundary defects. As calculated, the highest GND density of the Sample A is 3.5×10^{15} m^{-2}, while that of the Sample B is 7.3×10^{16} m^{-2}. Especially for the GND near the machined surface of Sample B, numbers of the dislocations entangled there and reach to the highest value, as marked in red dotted line in Fig. 8 (b). Compared to the Fig. 8 (a), there is no obvious GND density near the surface. Notably, in the Sample B, the GND density near the grain boundary is still high even if it is far away from the machined surface, as marked in the red dotted line. However, the GND density of the Sample A far away from the machined surface has significantly declined. Zhang et al. (2020) pointed that the high GND density would result in a partial increase of grain size, when grains grow to a certain extent, a process starts by emerging GND walls in grain interiors and ends by removing some GND at grain boundaries. Thus, combined with Fig. 4 and Fig. Fig. 8, the large grain size of the Sample B may attribute to the movement of GND. According to the analysis of GND, stress and temperature factors, partial recrystallization has occurred during the microcutting process with physiochemical effect. However, lack of adequate temperature generated by microcutting process make inner grains not recrystallized completely, and this area may be in the recovery stage. Additionally, the Schmid factor maps can also affirm that Schmid factor of the Sample B near the machined surface is close to 0.5, while the Schmid factor far away from the surface is smaller because there are high GND density in the grain, inhibiting recrystallization.

5. Conclusions

The physiochemical effect of surfactant on the microstructure of the microgroove in pure copper is studied. The conclusions are summarized as follows:

(1) There is an obvious reduction in machining forces in the sample with physiochemical effect during microcutting. The surface roughness of microgroove with physiochemical effect is 12 nm which is much lower than that without physiochemical effect (17 nm).

(2) On the cross-sectioned surface, the average grain size of the sample with physiochemical effect is 67.9 μm within the microgroove zone, and the grain size near the surface of microgroove is larger than that of ink-free microgroove. Additionally, the grain orientations of ink-affected surface present anisotropy, while that of ink-free surface are towards {101} direction.
(3) As the orientation distribution function maps shown, {110}<001>, {110}<112>, {111}<110> and {123}<634> textures dominate in the sample without physiochemical effect, and {110}<112>, {112}<111> and {124}<211> textures dominate in the sample with physiochemical effect.
(4) Based on the calculation and analysis, it can be inferred that the induced stress and temperature in the sample with physiochemical effect are higher than that without physiochemical effect, which can provide enough driving energy for recrystallization.

Declarations

Declaration of competing interest

The authors declare that they have no known competing financial interests or personal relationships that could have appeared to influence the work reported in this paper.

Acknowledgements

The authors express their gratitude to the financial support from the start-up fund of scientific research of Jiangxi University of Science and Technology (Grant No: 205200100544).

References

Yi, A.Y., Lu, W., Farson, D.F., Lee, L.J., 2008. Overview of polymer micro/nanomanufacturing for biomedical applications, Adv. Polym. Technol., 27, 188–198.

Tan, N.Y.J., Zhang, X., Neo, D.W.K., 2019. Ultra-precision diamond shaping of microchannels for microfluidic applications, In: 19th International conference of the European Society for Precision Engineering and Nanotechnology (euspen). Bilbao, Spain, 358–361.

Guo, J., Zhang, J., Wang, H., 2018. Surface quality characterisation of diamond cut V-groove structures made of rapidly solidified aluminium RSA-905, Precis. Eng, 53 120–133.

Otieno, T., Abou-El-Hossein. K., Hsu, W.Y., 2015. Surface roughness when diamond turning RSA 905 optical aluminium. In: Proc. SPIE, 957509.

Dornfield, D., Lee, D.E,.2008. Introduction to precision manufacturing. In: Dornfeld D, Lee D-E (eds) Precision Manufacturing, Springer US, Boston, MA, 1–33.

Sagapuram, D., Yeung, H., Guo, Y., Mahato, A., M'Saoubi, R., 2015. On control of flow instabilities in cutting of metals. CIRP Ann, 64 49–52.

Udupa, A., Viswanathan, K., Saei, M., Mann, J.B., Chandrasekar, S., 2018. Material-independent mechanochemical effect in the deformation of highly-strain-hardening metals. Physical Review Applied, 10, 014009.

Kramer, I.R., 1961. The effect of surface-active agents on the mechanical behavior of aluminum single crystals, Trans. AIME, 221, 989–993.

Roscoe, R., 1936, XXXII. The plastic deformation of cadmium single-crystals, London, Edinburgh, Dublin. Philos. Mag. J. Sci, 21, 399–406.

Rehbinder, P.A., 1928. On the effect of changes in the surface energy upon cleavage, hardness, and other crystal properties, In: The VI-th Congress of Russian Physicists, Moscow, 29.

Shaw, M.C., 1958. On the action of metal cutting fluids at low speeds, Wear, 2, 217–227.

Zhang, J., Lee, Y.J., Wang, H., 2021. Mechanochemical effect on the microstructure and mechanical properties in ultraprecision machining of AA6061 alloy. Journal of materials science and technology, 69, 228-238.

Wang, X.F., Guo, M.X., Cao, L.Y., Luo, J.R., Zhang, J.S., 2015. Effect of heating rate on mechanical property, microstructure and texture evolution of Al-Mg-Si-Cu alloy during solution treatment, Mater. Sci. Eng. A 621, 8-17.

Peirs, J., Tirry, W., Amin-Ahmadi, B., 2013. Microstructure of adiabatic shear bands in Ti6Al4V, Mater. Charact., 75, 79–92.

Zhang, J., Ma, M., Shen, F., 2018. Influence of deformation and annealing on electrical conductivity, mechanical properties and texture of Al-Mg-Si alloy cables, Mater. Sci. Eng. A., 710, 27–37.

Zhang, J., Lee, Y.J., Wang, H., 2021. Microstructure evaluation of shear bands of microcutting chips in AA6061 alloy under the mechanochemical effect, Journal of materials science and technology, 91, 178–186.

Zhang, J., Lee, Y.J., Wang. H., 2020. Surface Texture Transformation in Micro-Cutting of AA6061-T6 with the Rehbinder Effect. Int. J. of Precis. Eng. and Manuf.-Green Tech.

Shen, F., Yi, D., Wang, B., 2016. Semi-quantitative evaluation of texture components and anisotropy of the yield strength in 2524 T3 alloy sheets, Mater. Sci. Eng. A., 675, 386–395.

Zhang, J., Wang, B., Yi, D., 2019. Stress corrosion cracking behavior in 2297 Al–Cu–Li alloy at different grain orientations, Mater. Sci. Eng. A., 764, 138252.

Roland, B., Marek, B., Helmi, A., Philippe, P., Gilles, L., 2016. Chip formation and microstructure evolution in the adiabatic shear band when machining titanium metal matrix composites, Int. J .Mach. Tools. Manuf., 109, 137-146.

Chang, G., Miao, L., 2014. Adiabatic shear band of TC4 alloy during warm compression, Rare. Met. Mater. Eng., 43, 2069–2074.

Yin, W.H., Xu, F., Ertorer, O., 2013. Mechanical behavior of microstructure engineered multi-length-scale titanium over a wide range of strain rates, Acta Mater., 61, 3781–3798.

Guo, Y., Ruan. Q., Zhu S., 2019. Temperature Rise Associated with Adiabatic Shear Band: Causality Clarified, Phys. Rev. Lett., 122, 15503.

Liu, D., He, Y., Tang, X., Ding, H., Hu, P., 2012. Size effects in the torsion of microscale copper wires: experiment and analysis, Scr. Mater. 66, 406–409.

Nye, J.F., 1953. Some geometrical relations in dislocated crystals, Acta Metall. 1, 153–162.

Kröner, E., Balian, R., 1981. Physics of Defects, North-Holland, Amsterdam, 219–315.

Pantleon, W., 2008. Resolving the geometrically necessary dislocation content by conventional electron backscattering diffraction, Scr. Mater. 11, 994–997.

Zhang, J., Wang, B., Wang, H., 2020. Geometrically necessary dislocations distribution in face-centred cubic alloy with varied grain size, Mater. Charact., 162, 110205.

Figures

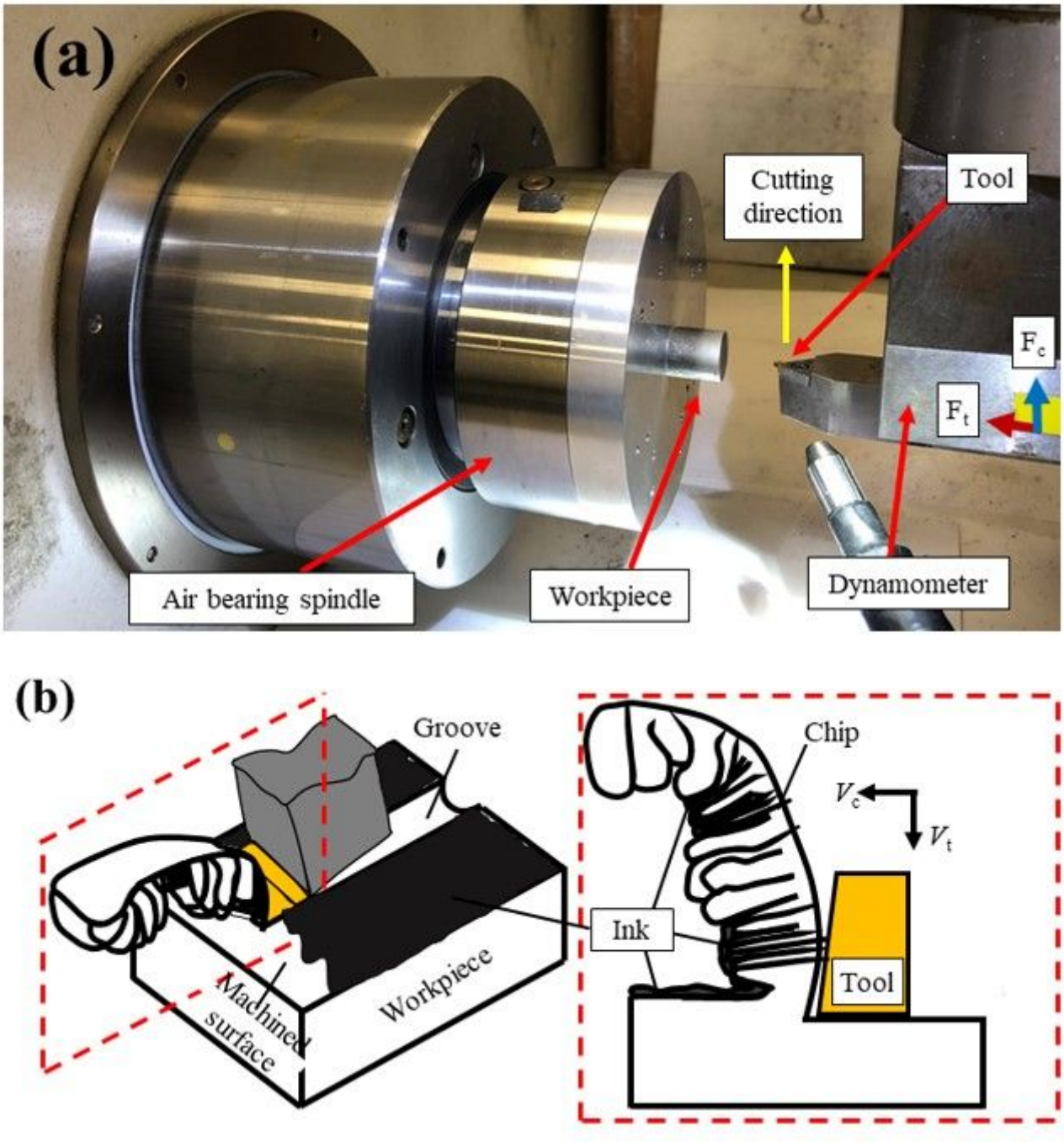

Figure 1

(a) Ultraprecision microcutting experimental device and (b) schematic diagram of microcutting (Zhang et al. 2021) (Fc and Ft are the cutting and thrust forces, respectively)

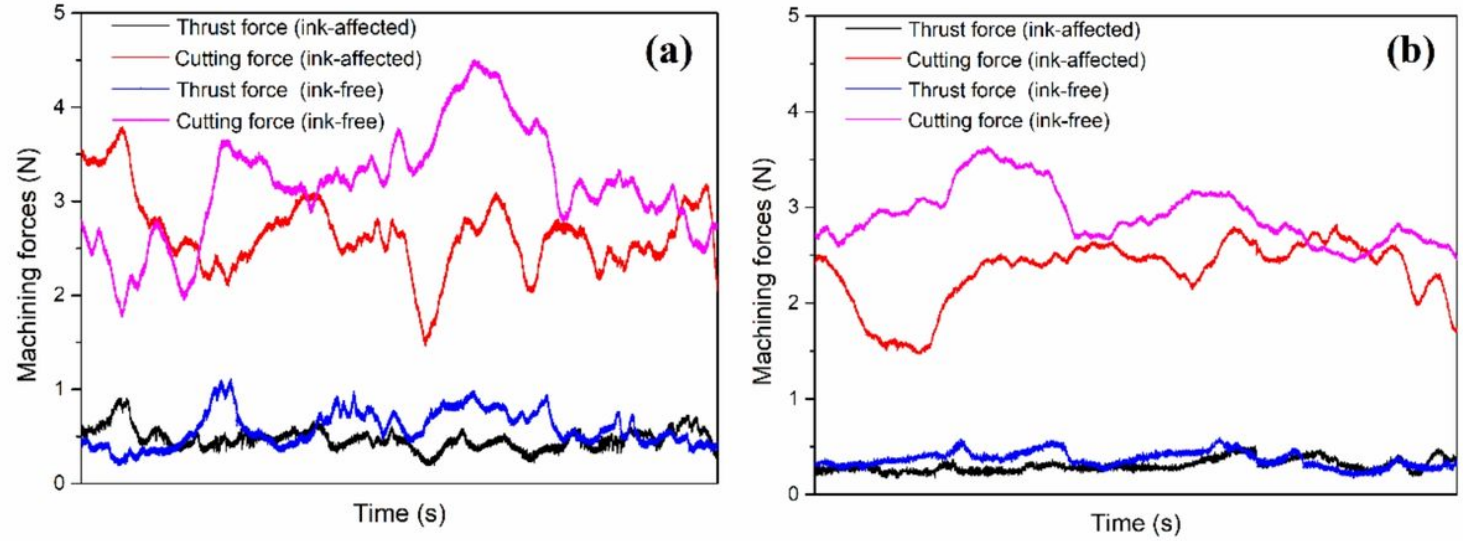

Figure 2

The tested machining forces of microgrooves during microcutting at different cutting parameters (a) cutting speed 25 mm/min and (b) cutting speed 100 mm/min

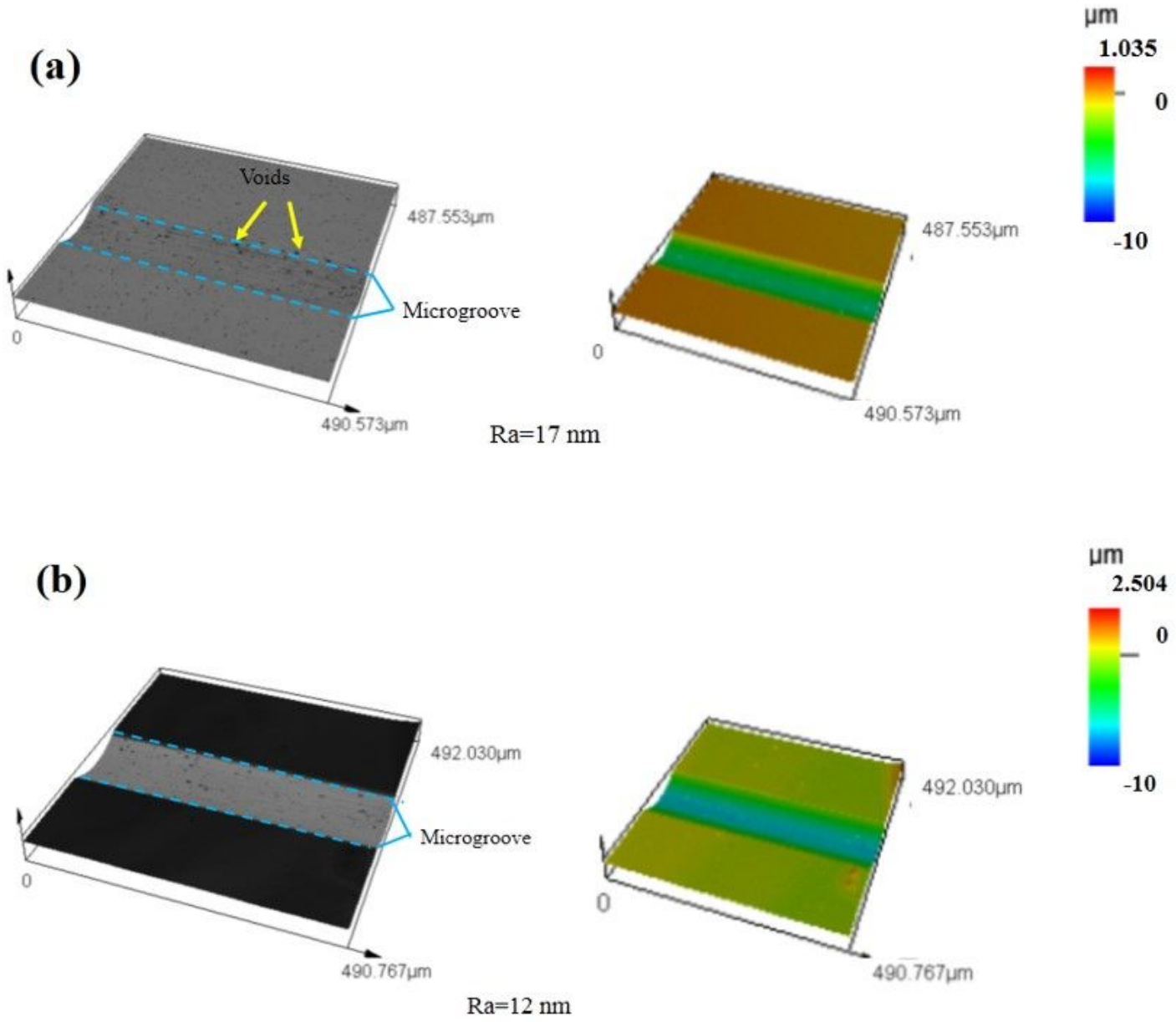

Figure 3

The laser scanned micrograph of the 10 μm microgrooves: (a) Sample A and (b) Sample B (Ra represents the most important evaluation parameter of surface roughness, arithmetic mean deviation).

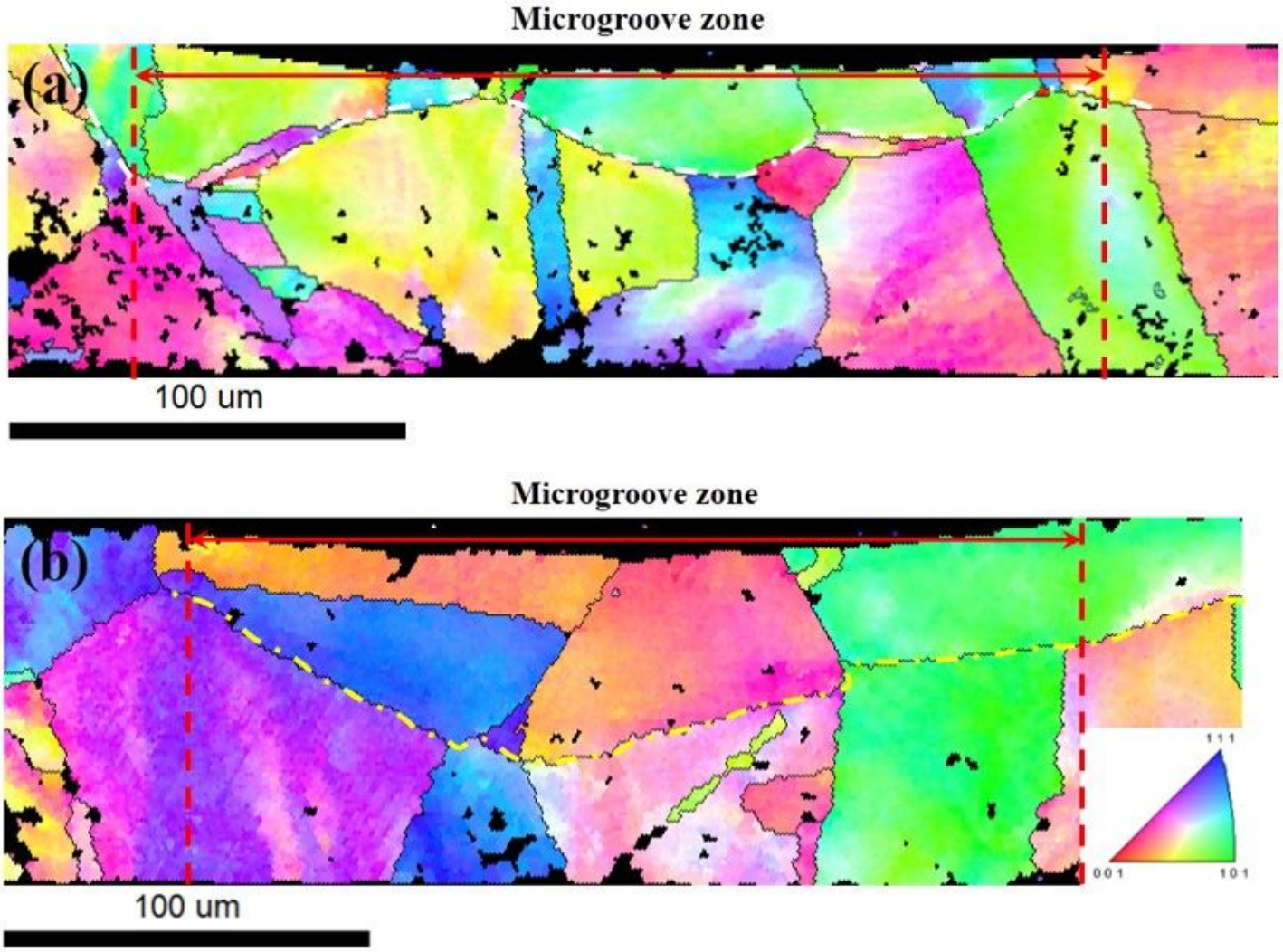

Figure 4

EBSD maps of the cross-sectioned microgrooves of (a) Sample A and (b) Sample B (with physiochemical effect), and inverse pole figure is inserted: red indicates {001}, blue for {111}, and green for {110} direction

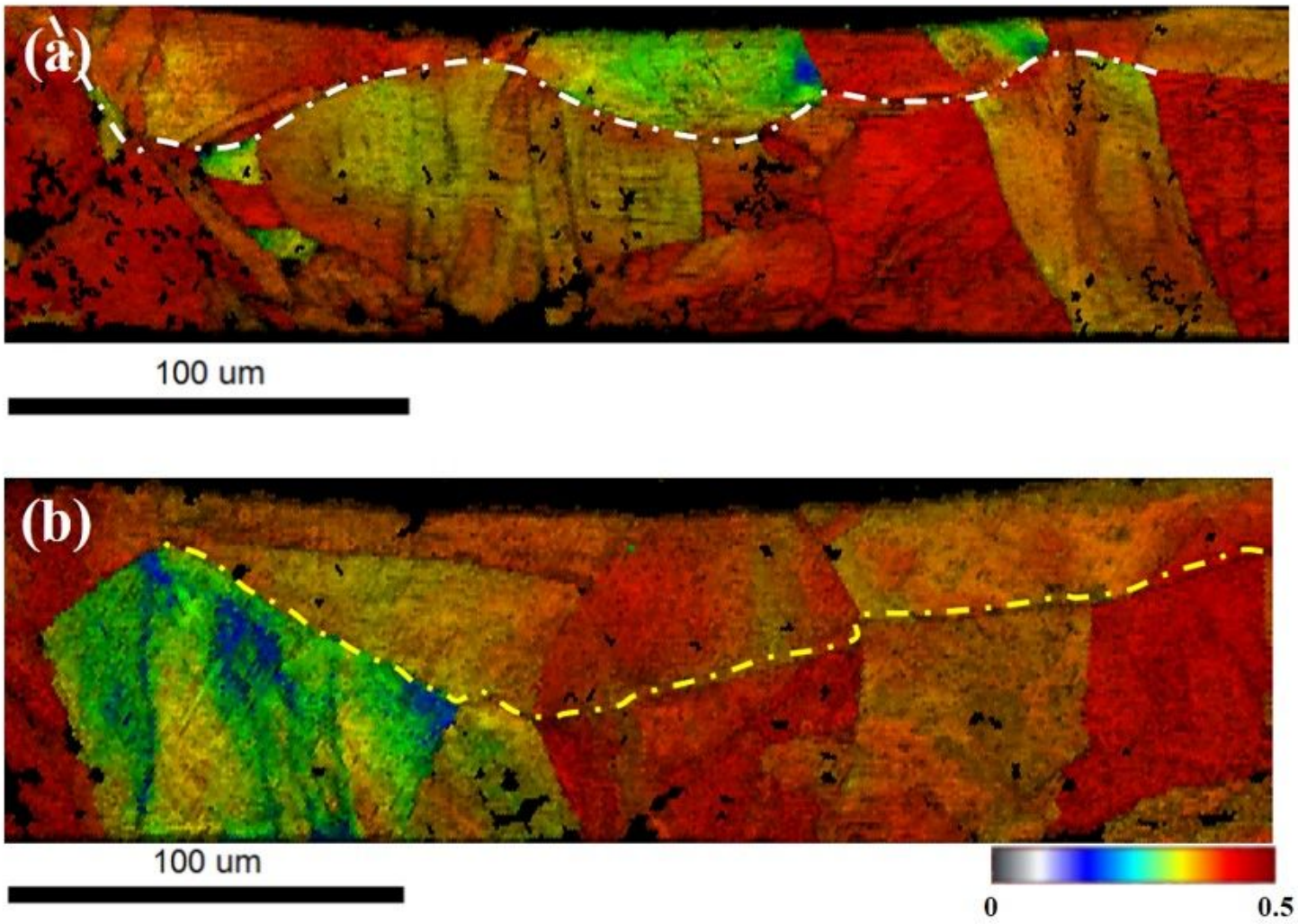

Figure 5

Schmid factor maps for grains in the cross-sectioned microgroove zones of (a) Sample A and (b) Sample B

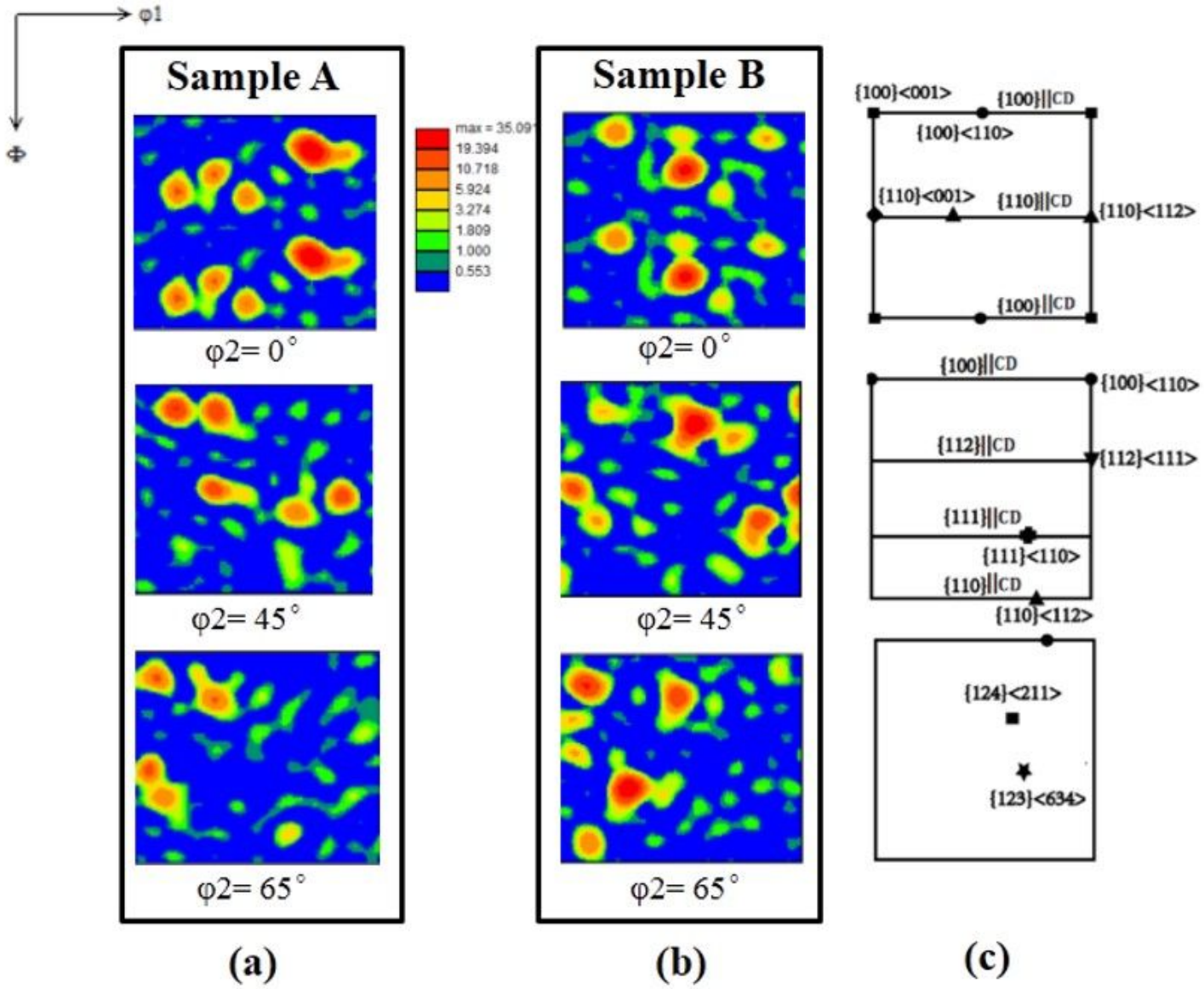

Figure 6

ODF maps for the cross-sectioned microgroove of (a) Sample A, (b) Sample B and (c) schematic structure of main textures in (φ1, Φ, φ2) (CD represents the cutting direction)

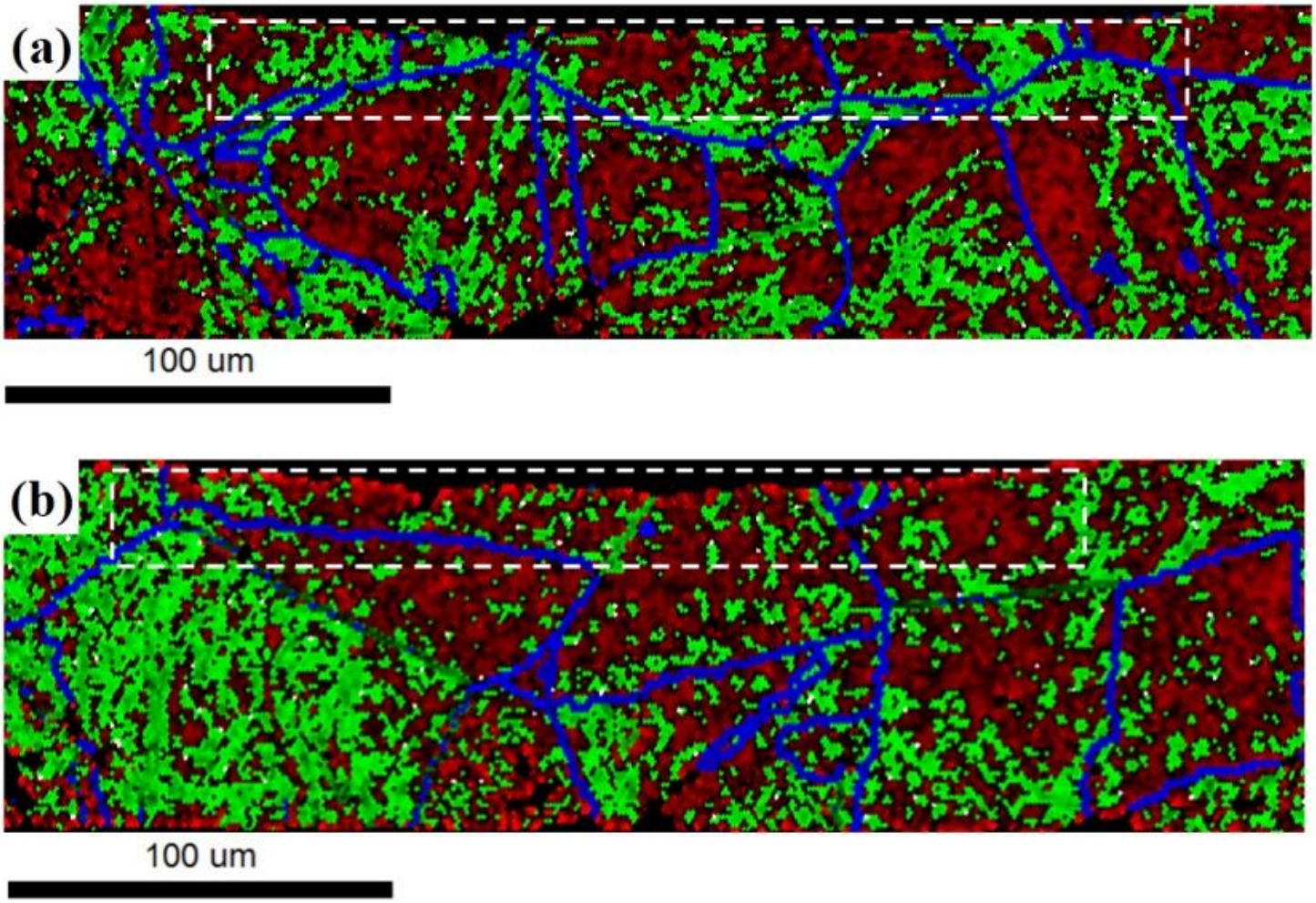

Figure 7

The average misorientation maps of the samples: (a) Sample A and (b) Sample B, showing the recrystallization degree (red regions represent HABs, green regions represent LABs and blue is the grain boundaries)

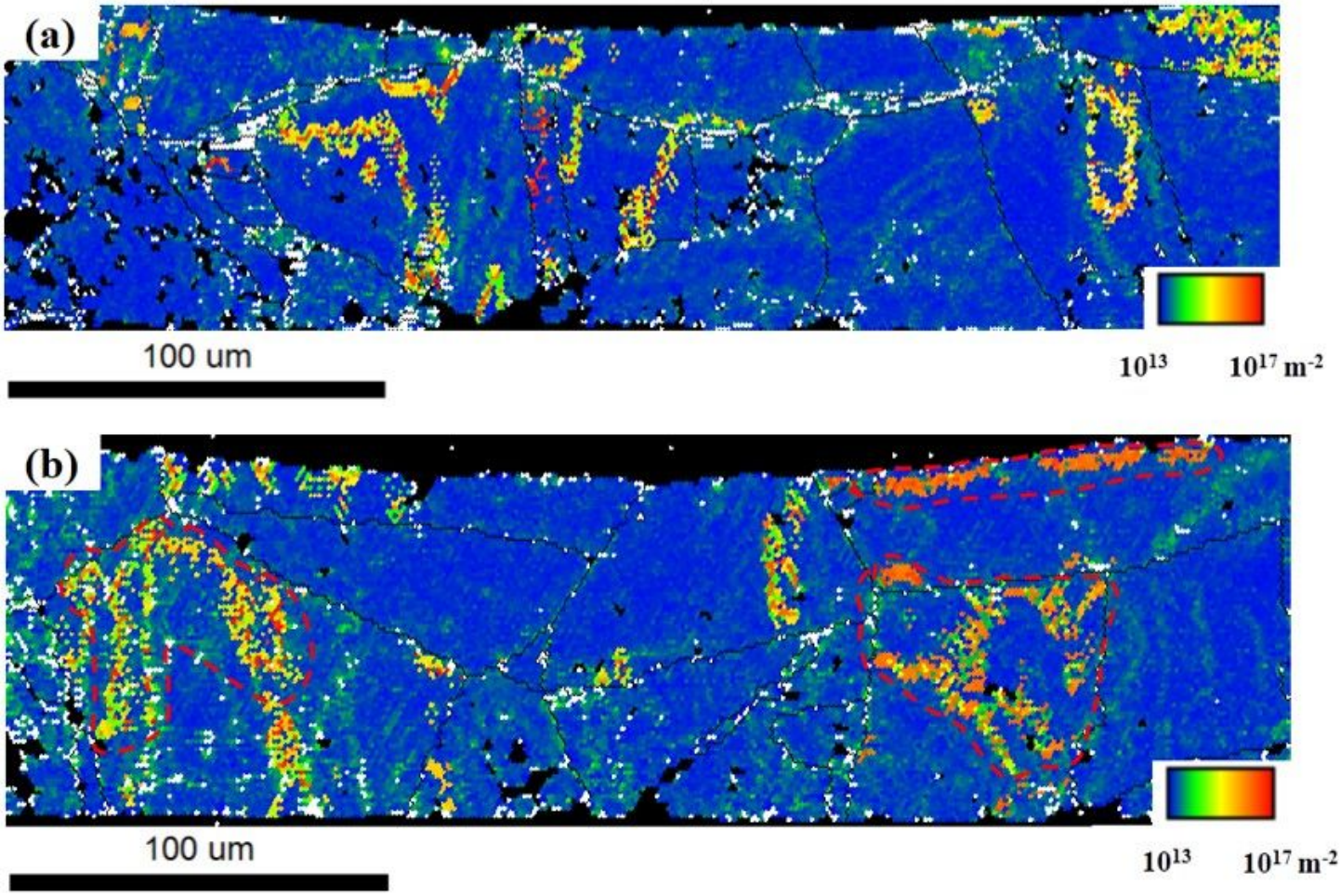

Figure 8

GND density distribution maps of the samples after microcutting: (a) Sample A and (b) Sample B (with physiochemical effect)